Astronomy & Astrophysics manuscript no. sample
February 28, 2024

Modeling effects of starspots on stellar magnetic cycles

Zebin Zhang[1,2], Jie Jiang[1,2], and Leonid Kitchatinov[3,4]

[1] School of Space and Environment, Beihang University, Beijing, China
e-mail: jiejiang@buaa.edu.cn
[2] Key Laboratory of Space Environment monitoring and Information Processing of MIIT, Beijing, China
[3] Institute of Solar-Terrestrial Physics, Irkutsk, Russia
[4] Pulkovo Astronomical Observatory, St. Petersburg, Russia

Received xx, 2023; accepted xx, 2023

ABSTRACT

Context. Observations show that faster-rotating stars tend to have stronger magnetic activity and shorter magnetic cycles. The cyclical magnetic activity of the Sun and stars is believed to be driven by the dynamo process. The success of the Babcock-Leighton (BL) dynamo in understanding the solar cycle suggests an important role that starspots could play in stellar magnetic cycles.
Aims. We aim at extending the BL mechanism to solar-mass stars with various rotation rates and explore the effects of emergence properties of starspots in latitudes and tilt angles on stellar magnetic cycles.
Methods. We adopt a kinematic BL-type dynamo model operating in the bulk of the convection zone. The profiles of the large-scale flow fields are from the mean-field hydrodynamical model for various rotators. The BL source term in the model is constructed based on the rotation dependence of starspots emergence. That is, faster rotators have starspots at higher latitudes with larger tilt angles.
Results. Faster rotators have poloidal flux appearing closer to about ±55° latitudes, where the toroidal field generation efficiency is the strongest because of the strongest latitudinal differential rotation there. It takes a shorter time for faster rotators to transport the surface poloidal field from their emergence latitude to the ±55° latitudes of efficient Ω-effect thus shortening their magnetic cycles. The faster rotators operate in a more supercritical regime due to a stronger BL α-effect relating to the tilt angles, which leads to stronger saturated magnetic fields and a coupling of the poloidal field between two hemispheres more difficult. Thus the magnetic field parity shifts from the hemispherically asymmetric mixed mode to quadrupole, and further to dipole when a star spins down.
Conclusions. The emergence of starspots plays an essential role in the large-scale stellar dynamo.

Key words. dynamo – stars: activity – stars: magnetic field – stars: starspots – stars: rotation

1. Introduction

The solar large-scale magnetic fields show the quasi-11-yr cyclic variations manifested by the sunspots (Hathaway 2015). Starspots and magnetic cycles are ubiquitous among cool stars (Strassmeier 2009; Boro Saikia et al. 2018). The progress in solar magnetism paves the way for the understanding of stellar activity (Brun et al. 2015).

The cyclical magnetic activity of stars is usually studied through the chromospheric emission, e.g., Ca II H&K emission (Wilson 1978) or photospheric brightness variations (e.g., Reinhold et al. 2017; Montet et al. 2017). These studies show a general P_{rot}–P_{cyc} relation, that is the magnetic cycle period P_{cyc} tends to be longer for stars having longer rotation period P_{rot} (Noyes et al. 1984b). Some studies show two branches of this relation, active and inactive ones corresponding to high and low activity, respectively (Saar & Brandenburg 1999; Böhm-Vitense 2007; Wright et al. 2011), while the existence of the active branch is still controversial (Boro Saikia et al. 2018). Past efforts on stellar activity also reveal the dependence of magnetic activity amplitude on the rotation period, hereafter called the P_{rot}–A_{cyc} relation. That is, younger and faster rotating stars tend to have higher magnetic activity amplitude A_{cyc}. When rotators are fast enough, magnetic activity amplitude tends to saturate at some level (Hempelmann et al. 1996; Güdel 2004; Wright & Drake 2016; Zhang et al. 2020).

The P_{rot}–P_{cyc} relation of stellar magnetism provides an important observational test for dynamo models. In kinematic α-Ω mean-field dynamo, the decreasing trend of the cycle period along the rotation period is a general property, because the cycle period is determined by the dynamo number related to the rotation period (Tobias 1998). During the past decades, the flux transport dynamo (FTD, Wang et al. 1991; Durney 1995; Choudhuri et al. 1995) works as the paradigm in understanding the solar cycle. In the framework of the FTD, the cycle period is controlled by the rate of meridional flow (Dikpati & Charbonneau 1999; Jouve & Brun 2007). If extending the FTD model to stars, the P_{rot}–P_{cyc} relation requires an increase of meridional flow as the rotation rate increases (Nandy 2004). But magnetohydrodynamic (MHD) simulations show that the strength of meridional flow decreases as stars rotate faster (Brown et al. 2008; Augustson et al. 2012). Thus the faster rotators host longer magnetic cycles (Jouve et al. 2010; Karak et al. 2014b), which is contrary to what is observed. Kitchatinov (2022) suggests that the effective temperature is the essential parameter in understanding stellar magnetic cycles. Hotter stars sustain shorter cycles and they rotate faster on average. Brun & Browning (2017) introduce muti-cell meridional flows to reconcile the discrepancy. Do Cao & Brun (2011) consider the effect of magnetic turbulent pumping, and found the magnetic cycle shortens when the pumping effect becomes stronger with the increase of rotation rate. Pipin & Kosovichev (2016) include the dynamical quenching of magnetic buoyancy and magnetic helicity and Hazra et al.

(2019) introduce near-surface pumping and assume the faster rotators have a stronger BL source term. They both reproduce the relation between rotation period and magnetic cycle close to observations. MHD simulations report a weak relation between the rotation period and magnetic cycle with a negative slope (Warnecke 2018; Strugarek et al. 2017; Brun et al. 2022), while Guerrero et al. (2019) find a trend of the increase of the magnetic cycle with the rotation period under some conditions.

The P_{rot}–A_{cyc} relation is another observational test for dynamo models. Faster rotators tend to form starspots with larger tilt angles, which could explain the P_{rot}–A_{cyc} relation in the framework of the BL mechanism. Sunspots are formed by the buoyant rise of subsurface toroidal flux (Parker 1955). The Coriolis force acts on the rising toroidal flux, leading to tilt angles of sunspot groups (Fan 2021). Starspots are expected to be formed in a similar process as sunspots. The Coriolis force increases for faster rotators and thus could lead to a larger tilt angle (Caligari et al. 1995; Işık et al. 2018). The tilt angles correspond to the strength of the BL source term, so faster rotators sustain a stronger BL source term. Based on the assumption that faster rotators sustain a stronger BL source term due to larger tilt angles, the P_{cyc}–A_{cyc} relation was reproduced by Karak et al. (2014b); Hazra et al. (2019). Furthermore, Kitchatinov & Olemskoy (2015) considered the saturation of the BL mechanism for the tilt angles approaching $\pi/2$ and reproduced the magnetic activity saturation for very fast rotators. Some MHD simulations have also been carried out to understand the scaling law between stellar magnetic activity and rotation period (Augustson et al. 2019; Brun et al. 2022).

Solar observations show that stronger cycles tend to have smaller tilt angles (Dasi-Espuig et al. 2010; Jiao et al. 2021), which influence the contribution of sunspots to the polar fields. The polar fields at cycle minimum are believed to be the source of the toroidal field of a new cycle, which determines the strength of the subsequent solar cycle (Muñoz-Jaramillo et al. 2013; Cameron & Schüssler 2015; Jiang et al. 2018). So the cycle-dependent tilt angles of sunspot emergence works as a nonlinear mechanism to modulate the amplitude of the solar cycle, which is called tilt quenching. Observations also show that stronger cycles tend to have sunspot emergence at higher latitudes (Li et al. 2003; Solanki et al. 2008; Jiang et al. 2011). The higher latitudes the sunspots emerge, the weaker their contribution to build up the polar fields (Jiang et al. 2014a; Petrovay et al. 2020). So the cycle-dependent latitudes of sunspot emergence is another nonlinear feedback for the solar cycle, which is called latitude quenching. Systematic studies on the both forms of quenching have demonstrated that they play a crucial role in modulating the amplitude of the solar magnetic cycle (Jiang 2020; Karak 2020; Talafha et al. 2022). This raises an interesting question of how the starspots' emergence latitudes and tilt angles influence stellar magnetic cycles.

Sunspots appear only at latitudes lower than about 40°. But for starspots, the emergence latitudes could be distributed over the whole stellar disk (Strassmeier 2009). Observations also show faster rotators tend to have starspots at higher latitudes and even at polar regions (Vogt & Penrod 1983; Strassmeier et al. 1991). For the first time Schuessler & Solanki (1992) suggested an origin of the polar starspots, which result from a dominance of the Coriolis force in the dynamics of magnetic flux tubes emergence. Işık et al. (2018) calculate the emergence latitudes and tilt angles of starspots for various rotators, then apply the surface flux transport model to understand the evolution of the large-scale field at stellar surfaces. They found that faster rotators with starspots at higher latitudes reverse the polarity of the polar field in a shorter time, which implies faster rotators have shorter magnetic cycles. This work also inspires us to explore the effects of emergence properties of starspots on stellar magnetic cycles in the BL-type dynamo framework.

Zhang & Jiang (2022) recently develop a new generation of the BL-type dynamo model operating in the bulk of the convection zone, rather than in the tachocline. The model establishes a global dipolar fields connecting two solar poles. The configuration of the near surface poloidal field is consistent with observations and differs from most other available dynamo models. The poloidal field is sheared by latitudinal differential rotation and generate the strong toroidal field in the bulk of the convection zone as the source of sunspots. The tachocline is not important in their model, which is supported by stellar observations and MHD simulations that the dynamo process is more likely to operate in the bulk of the convection zone (Nelson et al. 2013; Yadav et al. 2015; Wright & Drake 2016).

This work aims at extending the solar dynamo model of Zhang & Jiang (2022) to stars with a solar mass ($M_\odot$), ranging the rotation periods from 10 to 25 days, and explore the effect of starspots emergence properties on magnetic cycles, and further test if the P_{rot}–P_{cyc} and P_{rot}–A_{cyc} relations can be reproduced due to starspots' properties. On the other hand, the tests of stellar observations could also verify the solar dynamo model. We will quantify the dependence of starspots' emergence properties in tilt angles and latitudes on the rotation rate of stars based on observations.

The paper is organized as follows. The BL-type dynamo model is described in Sect. 2. We determine the critical dynamo number in Sect. 3.1.1. The effect of the emergence latitude of starspots on the magnetic cycle is explored in the linear regime in Sect. 3.1.2. The P_{cyc}–A_{cyc} relation is studied in the nonlinear regime in Sect. 3.2. We summarize our results in Sect. 4.

2. MODEL

In this study, we adopt the kinematic dynamo model developed by Zhang & Jiang (2022), who deal with the evolution of axisymmetric large-scale magnetic field, $\mathbf{B}(r,\theta,t) = B(r,\theta,t)\hat{\mathbf{e}}_\phi + \nabla\times\left[A(r,\theta,t)\hat{\mathbf{e}}_\phi\right]$, with prescribed flow profiles in the standard spherical polar coordinates (r,θ,ϕ). The dynamo equations are expressed as

$$\frac{\partial A}{\partial t} + \frac{1}{s}[(\mathbf{u}_p + \gamma_r\hat{\mathbf{e}}_r)\cdot\nabla](sA) = \eta\left(\nabla^2 - \frac{1}{s^2}\right)A + S_{BL}, \tag{1}$$

$$\frac{\partial B}{\partial t} + \frac{1}{r}\left[\frac{\partial(u_r+\gamma_r)rB}{\partial r} + \frac{\partial(u_\theta B)}{\partial\theta}\right] = \eta\left(\nabla^2 - \frac{1}{s^2}\right)B + s(\mathbf{B}_p\cdot\nabla\Omega) + \frac{1}{r}\frac{d\eta}{dr}\frac{\partial(rB)}{\partial r}, \tag{2}$$

where η and γ_r represent the turbulent diffusivity and the radial pumping, respectively. Differential rotation and meridional flow are represented by $\Omega(r,\theta)$ and $\mathbf{u}_p(r,\theta) = u_r(r,\theta)\hat{\mathbf{e}}_r + u_\theta(r,\theta)\hat{\mathbf{e}}_\theta$, respectively. The parameters will be presented in the next subsections.

2.1. Differential rotation and meridional flow

The large-scale flows in $1M_\odot$ stars rotating with different rates are specified with the method developed by Kitchatinov & Rüdiger (1999). The mean-field model based on this method

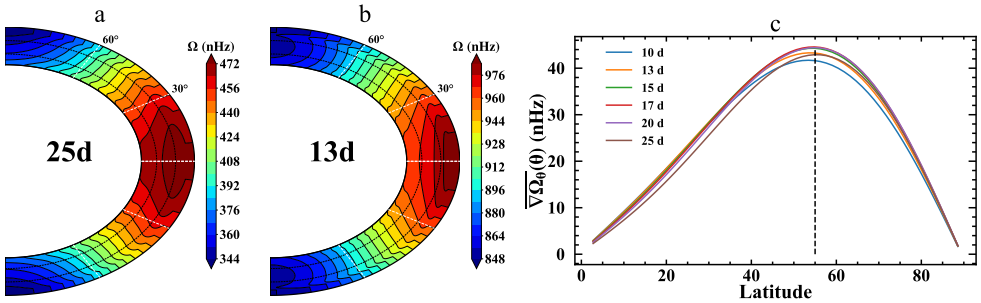

Fig. 1. Differential rotations of solar-mass stars. Panels (a) and (b) are the profiles of differential rotation for stars with rotation periods of 25 and 13 days, respectively. Panel (c) shows the latitudinal distribution of the radius-averaged latitudinal shear $\overline{\nabla\Omega_\theta}(\theta)$ for the different rotators we study. The vertical dashed line denotes 55° latitude.

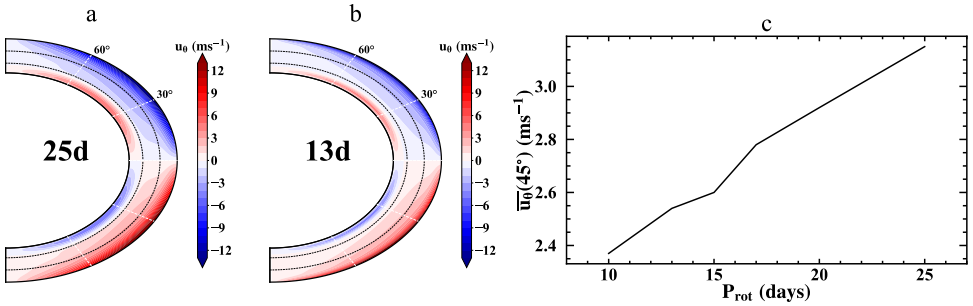

Fig. 2. Meridional flows of solar-mass stars. Panels (a) and (b) are the latitudinal component of the meridional flow patterns for the stars with rotation periods of 25 and 13 days, respectively. Panel (c) shows the dependence of the averaged return flow at 45°, $\overline{u_\theta}(45°)$, on the stellar rotation period.

(Kitchatinov & Olemskoy 2011, 2012) predicts the dependence of differential rotation on the spectral type and rotation rate in agreement with observations by Barnes et al. (2005) and Balona & Abedigamba (2016). Here, the version of the differential rotation model by Kitchatinov & Nepomnyashchikh (2017b) adapted for using in dynamo simulations is applied. The results have been adopted to understand properties of the stellar magnetic field (e.g. Hazra et al. 2014; Kitchatinov 2022). Observations indicate that faster rotators tend to have stronger torsional oscillations (Collier Cameron & Donati 2002) and more irregular stellar cycles (Baliunas et al. 1995; Boro Saikia et al. 2018). Hence we restrict our computations to slowly rotating $1M_\odot$ stars with the rotation periods from 10 to 25 days.

Figures 1 (a) and (b) show the profiles of differential rotation for stars with sidereal rotation periods of 25 and 13 days, respectively. The former one corresponds to the solar case and is close to helioseismic results (Schou et al. 1998). With the increase of the rotation rate, the differential rotation changes toward a cylinder-shaped pattern. It is the latitudinal shear in the bulk of the convection zone that winds the poloidal field for the dynamo model we use. Figure 1 (c) shows the latitudinal distribution of the latitudinal shear, $\overline{\nabla\Omega_\theta}(\theta) = 2\pi \int_{0.72R_\odot}^{R_\odot} \nabla\Omega_\theta(r,\theta)\, dr$. With the increase of the rotation rate, the strength of latitudinal shear increases slightly, which is consistent with observations (Barnes et al. 2005). Similar to the Sun, all stars have the strongest latitudinal shear at about ±55° latitude, where the generation efficiency of the toroidal field is the strongest and corresponds to the seat of stellar dynamo processes (Zhang & Jiang 2022).

Figures 2 (a) and (b) show the θ component of the meridional flow, u_θ, for stars with rotation periods of 25 and 13 days, respectively. For all rotators, the flow has a single-cell structure in each hemisphere, and is poleward near the surface and equatorward at the bottom of the convection zone. Figure 2 (c) shows the dependence of the equatorward return flow, $\overline{u_\theta}(45°)$, on the rotation period. The radius-averaged return flow, $\overline{u_\theta}(\theta)$, is defined as $\overline{u_\theta}(\theta) = \int_{0.72R_\odot}^{R_c} u_\theta(r,\theta)\, dr / \int_{0.72R_\odot}^{R_c} dr$, where R_c is the depth that the equatorward flow starts for different rotators. The strength of $\overline{u_\theta}(45°)$ decreases from 3.15 m s^{-1} to 2.4 m s^{-1} with the decrease of the rotation period from 25 days to 10 days. This trend is consistent with 3-D convective simulations (Brown et al. 2008; Augustson et al. 2012). The slower return flow for faster rotators is the reason why the FTD dynamo models failed to reproduce observational P_{rot}–P_{cyc} relation (Karak et al. 2014b).

2.2. Turbulent pumping and diffusivity

A near-surface radial pumping γ_r is included in our model aiming at matching the observed large-scale magnetic field evolution at the solar surface (Cameron et al. 2012; Jiang et al. 2013). We adopt its profile as

$$\gamma_r(r) = -\frac{\gamma_0}{2}\left[1 + \mathrm{erf}\left(\frac{\mathrm{r} - \mathrm{r_s}}{\mathrm{d_s}}\right)\right], \tag{3}$$

where $r_s = 0.9R_\odot$ and $d_s = 0.01R_\odot$ making sure that the pumping is confined near surface and smoothly decreases to zero at $0.88R_\odot$. A large enough γ_0 near surface is used just to prevent the diffusive escape of magnetic flux through the solar surface. Its amplitude and penetration depth are free parameters and has no effect on the cycle period of the dynamo model. Here we set $\gamma_0 = 20$ m s^{-1} for all rotators.

Turbulent diffusivity η within the stellar convection zone is still poorly constrained. Assuming that the turbulent convection dominates η in the convection zone and it gets significantly reduced through the overshot layer. We adopt the following diffu-

sivity profile

$$\eta = \frac{\eta_{cz}}{2}\left[1 + \mathrm{erf}\left(\frac{\mathrm{r} - \mathrm{r_c}}{\mathrm{d_c}}\right)\right] + \frac{\eta_s}{2}\left[1 + \mathrm{erf}\left(\frac{\mathrm{r} - \mathrm{r_s}}{\mathrm{d_s}}\right)\right], \quad (4)$$

where $r_c = 0.7R_\odot$ and $d_c = 0.03R_\odot$ correspond to the center and thickness of the overshot layer. The turbulent diffusivity in the bulk of the convection zone η_{cz} is taken as $3.7{\times}10^7$ m^2 s^{-1}, which is closer to the value estimated by the mixing-length theory than most values used by FTD models (see Figure 1 of Muñoz-Jaramillo et al. 2011). The diffusivity near the surface η_s is taken as the supergranular diffusivity 3.0×10^8 m^2 s^{-1}, which is within the range of observational studies summarized in Table 1 of Schrijver et al. (1996).

2.3. Babcock-Leighton source term

The BL-type source term shown in Eq.(1) is the core of the model setup to achieve our main objective of exploring the influence of starspots' emergence characteristics on stellar magnetic cycles. It is defined as

$$S_{BL}(r, \theta, t) = \alpha(r, \theta)\bar{B}(\theta, t). \quad (5)$$

The poloidal field is produced from the mean toroidal field $\bar{B}(\theta, t)$ in the bulk of the convection zone from $0.72R_\odot$ to $0.88R_\odot$, i.e.,

$$\bar{B}(\theta, t) = \int_{0.72R_\odot}^{0.88R_\odot} B(r, \theta, t) r dr \Big/ \int_{0.72R_\odot}^{0.88R_\odot} r dr, \quad (6)$$

where 0.72 $R_\odot$ and 0.88 $R_\odot$ corresponds to the inner boundary and penetration depth of the pumping, respectively.

The α-effect term can be written as

$$\alpha(r, \theta) = \frac{\alpha_0}{2} g(r) f(\theta). \quad (7)$$

The radial dependence of the α-effect is to constrain the BL process just working near the surface based on the essence of the BL process. It is rewritten in the form

$$g(r) = \left[1 + \mathrm{erf}\left(\frac{\mathrm{r} - \mathrm{r}_\alpha}{\mathrm{d}_\alpha}\right)\right], \quad (8)$$

where $r_\alpha = 0.95R_\odot$ and $d_\alpha = 0.01R_\odot$.

To explore how the latitudes of starspots emergence influence magnetic cycles, we design the $f(\theta)$ term as

$$f(\theta) = \frac{\cos\theta \sin^n\theta}{Max[\cos\theta \sin^n\theta, \theta \in (0, \pi)]}, \quad (9)$$

where $\cos\theta$ reflects the latitude dependence of the tilt angles caused by the Coriolis force and $Max[\cos\theta \sin^n\theta, \theta \in (0, \pi)]$ keeps the maximum value of Eq. (9) the same for the various n values. The factor $sin^n\theta$ reflects the dependence of the probability of toroidal flux emergence on latitude (Cameron & Schüssler 2017). We suppose a linear relation between the rotation period P_{rot} of stars and the n value,

$$n = 1 + (P_{rot} - 10) * 0.55, \quad (10)$$

so that it is $n = 1$ for $P_{rot} = 10$ days and $n = 9.25$ for $P_{rot} = 25$ days. With the decrease of rotation rate, the n value increases and constrains the emergence of starspots to lower latitudes. Figure 3 shows latitudinal variations of Eq. (9) for various rotators. As stars rotate faster, n decreases and the maxima of the curves shift to higher latitudes. For the rotation period from 25 days to 10 days, the latitude of maximum α changes from 18° to 45°.

Note that Eq. (10) is formulated to mimic the observation of faster rotators displaying starspots at higher latitudes, which are nearer to ±55° latitudes. The trend is in agreement with the thin-flux-tube simulations by Işık et al. (2018), who utilized a surface flux transport model to investigate stellar brightness variations for different levels of magnetic activity and rotation rates. To date, neither observations nor numerical simulations have been able to determine the exact dependence of starspots' latitudes on P_{rot}. We will also consider a quadratic relationship between n and P_{rot}, that is $n = 9.25(P_{rot}/P_{sun})^2$, and independence of n on the rotation period, that is $n = 1$ in Eq. (10) as a contrast, in Sect. 3.1.

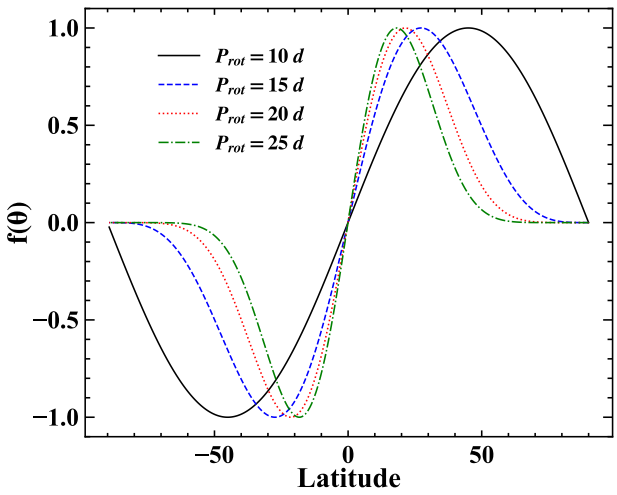

Fig. 3. Latitude variation of the α profiles determined by Eq. (9) for stars with different rotation periods.

Another important parameter of the BL source term is its strength α_0, dominated by tilt angles of starspots. The dynamo number, $\alpha_0 \Delta\Omega R^3/\eta^2$, is a key parameter in the dynamo process. It describes the efficiency of magnetic fields generation versus decay caused by diffusion. A self-sustained dynamo process occurs when the dynamo number exceeds a critical value. After given a specific profile of diffusivity, differential rotation and the source term of the poloidal field, the strength of the dynamo number is determined by the free parameter α_0 in Eq. (7). So that a non-decay dynamo process occurs when α_0 is greater than or equal to its critical value α_c. In most previous dynamo models, α_0 was determined arbitrarily. Kitchatinov & Nepomnyashchikh (2017a) (hereafter KN17) suggest that α_0 could be constrained based on observations.

KN17 assumes that the upper bound P_{max} for the rotation period of solar-type stars (van Saders et al. 2016) corresponds to near marginal dynamo excitation. In other words, the faster-rotating stars tend to have a stronger α-effect and operate in a more supercritical regime. For the BL mechanism, α_0 is dominated by the tilt angles. The Coriolis force is stronger for faster rotators, thus leading to a larger tilt angle of starspots and then larger α_0. The $\alpha_0 - \alpha_c$ describes how supercritical the dynamo is. Motivated by KN17, we give α_0 for a star with the rotation period P_{rot} based on

$$\alpha_0 = (1 + m\frac{P_{max}}{P_{rot}})\alpha_c, \quad (11)$$

where m is a free parameter constraining the amount of supercriticality. We take P_{max} as 28 days for the solar-mass stars we study.

The saturated unsigned toroidal flux within the convection zone is around 10^{23} Mx for the solar case (Cameron & Schüssler 2015). The flux puts a constraint on the m value, which is taken as $m = 0.2$. This entails that supercriticality varies from about 20% to 56 % for rotators with P_{rot} from 25 to 10 days.

2.4. Initial and boundary conditions

The configuration of large-scale magnetic fields in the Sun and stars can be classified as equatorially symmetric (quadrupolar) and anti-symmetric (dipolar) parity. The latter one is the dominant parity in the Sun, while some observations imply that fast rotators might have dominant quadrupolar fields (Kochukhov 2021). In this work, we start the simulations with two kinds of seed magnetic fields, whereas the toroidal field is set to be

$$B(r,\theta)|_{t=0} = \sin(2\theta)\sin[\pi(r-0.72R_\odot)/0.28R_\odot] \quad (12)$$

for dipolar parity, or

$$B(r,\theta)|_{t=0} = \sin(\theta)\sin[\pi(r-0.72R_\odot)/0.28R_\odot] \quad (13)$$

for quadrupolar parity. The poloidal field is set to be zero.

The outer boundary condition satisfies the vertical field condition based on the constraint by Cameron et al. (2012). Accordingly, we use $\partial(rA)/\partial r = 0$, $B = 0$ at $r = R_\odot$. The inner boundary matches a perfect conductor, which means that $A = 0$, $\partial(rB)/\partial r = 0$ at $r = 0.72R_\odot$. At poles, $A = B = 0$. The computational domain of our model is $0.72R_\odot \le r \le R_\odot, 0 \le \theta \le \pi$. Note again that our model does not include the tachocline.

Our model is calculated using a code that utilizes the Crank-Nicolson scheme and an approximate factorization technique (van der Houwen & Sommeijer 2001). The code developed at Beihang university has been validated against the open-source Surya developed by A.R. Choudhuri and his colleagues (Chatterjee et al. 2004) and dynamo benchmark (Jouve et al. 2008).

3. Results

For the onset of dynamo instability, controlling parameters should exceed a certain critical value. The α_0 of Eq.(7) is the only variable parameter in our model since other parameters involved in the dynamo number, i.e., differential rotation and turbulent diffusivity, are given. Here we will first look for α_c for the dipolar and quadrupolar solutions and analyze properties of different symmetric solutions for different stars in Sect. 3.1. Then we will use the constrained α_0 given by Eq. (11) to analyze the dynamo behaviors of different stars in Sect. 3.2.

3.1. Linear model

3.1.1. Critical α-values, α_c, for dipolar and quadrupolar modes

With the time-independent large-scale flows and α independent of the magnetic field, dynamo Eqs. (1) and (2) are fully linear. Thus both A and B have exponential time dependence in the form of $e^{\lambda t}$, with $\lambda = \sigma + i\omega$. The real part σ is a growth rate, and the imaginary part ω is an oscillation frequency satisfying $\omega = \frac{2\pi}{P_{cyc}}$. The solution with zero linear growth rate ($\sigma = 0$) is the purely oscillatory one. The corresponding α_0 is the critical value denoted as α_c. Usually, α_c is derived as an eigenvalue problem of the linear system (e.g., Jiang & Wang 2006; Bonanno et al. 2002; Jiang & Wang 2007). Here we solve the dynamo equations as an initial value problem. With a given initial condition, we try different α_0 values. The larger α_0 value is, a faster grow rate σ is. The α_c is pinned down when $|\sigma| < 10^{-3}$ measured by the grow rate of the toroidal field integrated through the convection zone. In the linear system, the parity of fields is determined by the seed initial fields. For example, the seed fields with a pure dipolar parity could only excite a dipole-mode solution. So we use initial fields of dipolar (Eq. (12)) and quadrupolar (Eq. (13)) parity to find the critical values α_c^d and α_c^q for dipolar and quadrupolar parity, respectively.

Figure 4 shows α_c as a function of the stellar rotation period. For the Sun (sidereal rotation period about 25 days), α_c^d and α_c^q are 0.08 m s^{-1} and 0.18 m s^{-1}, respectively. The solution of dipolar parity has the smaller α_c, which means that the dipolar parity is easier to excite. This is consistent with the observed solar magnetic field, which is dominated by the dipolar field. Incidentally, α_c for the kinetic helicity at the base of the solar convection zone is about 10 m s^{-1} based on the estimation of Charbonneau (2020). Furthermore, Figure 4 shows that α_c increases with the rotation rate. The increase rate of the dipolar solutions (in the solid curve) differs from the quadrupolar one (in the dashed curve). The rotation period of 18 days marked a turning point. The dipolar (quadrupolar) solution prevails when the stellar rotation period is longer (shorter) than 18 days. Larger α_c indicates stronger diffusive annihilation of magnetic fields for a given system. The next subsection, especially Figure 6, will show that slower rotators have a simpler configuration of the magnetic field corresponding to lower order multipoles, which entails weaker diffusive annihilation (Wang & Sheeley 2002).

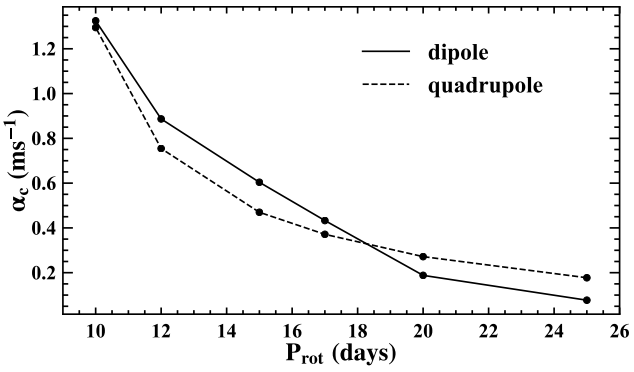

Fig. 4. Critical α-value, α_c, as a function of stellar rotation period (P_{rot}). The solid (dashed) curve represents the dipolar (quadrupolar) parity solution.

3.1.2. $P_{rot} - P_{cyc}$ relation and parity property

Figure 5 gives the relation between the rotation period and the magnetic cycle near marginal dynamo excitation. The solid (dashed) curve represents the dipolar (quadrupolar) solutions, both of which show that the magnetic cycle generally increases with the rotation period.

To understand what dominates the magnetic cycles in our model, we investigate the dependence of P_{cyc} on two parameters, the average speed of return meridional flow $\overline{u_\theta}$ and the critical number α_c. It turns out that $P_{cyc}^d \propto \overline{u_\theta}^{2.4}$ and $P_{cyc}^q \propto \overline{u_\theta}^{2.0}$. When the meridional flow is faster, the magnetic cycle is longer.

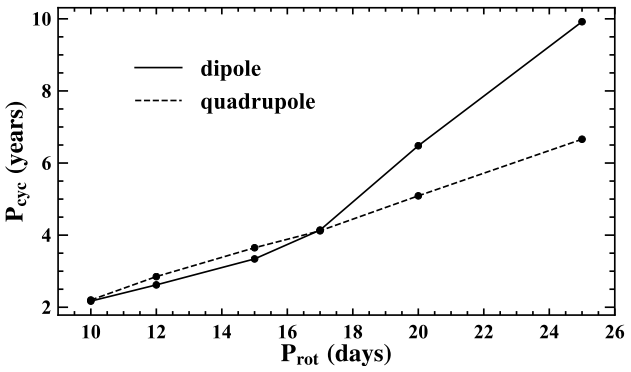

Fig. 5. Relation between rotation period (P_{rot}) and magnetic cycle (P_{cyc}). The solid (dashed) curve represents the dipolar (quadrupolar) parity solution.

This indicates that our model is different from the FTD models, in which the relation between P_{cyc} and $\overline{u_\theta}$ obeys $P^d_{cyc} \propto \overline{u_\theta}^x$, where $x = -0.89$ given by Dikpati & Charbonneau (1999) and $x = -0.696$ given by Karak (2010). On the other hand, it suggests $P^d_{cyc} \propto (\alpha^d_c)^{-0.79}$ and $P^q_{cyc} \propto (\alpha^q_c)^{-0.91}$. The magnetic cycle decreases with α_c and hence with the dynamo number. Faster rotators have a higher efficiency of dynamo process and then sustain a shorter magnetic cycle. In all simulations, we keep the pumping term the same. In models with turbulent pumping through the whole convection zone, the flux transport by pumping influences the cycle period (Guerrero & de Gouveia Dal Pino 2008; Hazra & Nandy 2016). The near-surface pumping introduced in our model only makes the surface part of the dynamo process consistent with observations (Cameron et al. 2012; Jiang et al. 2013). It does not affect the cycle period.

To further explore why faster rotators have a shorter magnetic cycle period, we plot the time evolution of dipolar (quadrupolar) magnetic fields for $P_{rot} = 10$ days in the first (third) row of Fig. 6. Figure 6 (a) shows that the poloidal flux relating to starspots emergence first appears around ±55° latitudes, where the latitudinal shear is the strongest. Therefore the newly generated poloidal flux could be sheared efficiently, thus generating the toroidal field for the subsequent cycle. The quick production of the toroidal field at high latitudes can be seen from Figs. 6 (b) - (c). Then the toroidal field gives rise to the poloidal field as illustrated by the dashed poloidal magnetic field lines in Fig. 6 (d). Thus a new magnetic cycle starts. The subsequent evolution of the poloidal field reverses the poloidal flux system of the old cycle. High-latitude starspots emergence shorten the dynamo process and hence the magnetic cycle.

As a comparison, we show the corresponding results of the solar case with $P_{rot} = 25$ days in the second row of Fig. 6. Figure 6 (e) shows that the newly generated poloidal flux at surface first appears around ±35° latitudes, which results from the setup of $n = 9.25$ in Eq.(9) to mimic the observation that sunspot emergence of each new cycle start from about ±35°. Then the poloidal flux is transported poleward, equatorward, and inward simultaneously. The surface turbulent diffusion leads to the equatorward migration, so that the net flux of one polarity resulting from the tilt angle diffuses across the equator. And this helps to finally establish the global dipolar field as shown in Fig. 6 (g). The poleward meridional flow along with the turbulent diffusion poleward transports the net flux of the other polarity to higher and higher latitudes. After a time interval Δt_1, they are transported to around the ±55° latitudes, where the latitudinal shear is the strongest, and the poloidal field is transported to a deeper depth by the inward turbulent diffusion as well. Thus the toroidal field of a new cycle first appears around ±55° (see Fig. 6 (f)). These toroidal fields could correspond to the ephemeral regions observed in the Sun (Zhang & Jiang 2022). The lower latitudes have a weaker latitudinal rotational shear, and hence it takes more time to wind up the poloidal field to generate the strong enough toroidal field for sunspot emergence of a new cycle. During the wind-up process, the newly generated weak toroidal field is transported to lower latitudes due to the effect of the equatorward return flows, which entails further more time to be wound up to generate the strong enough toroidal field. So that the toroidal field of the new cycle is gradually built up at the lower latitudes as demonstrated by Figs. 6 (f)-(h). We denote the time delay caused by the latitude dependence of the latitudinal shear as Δt_2. Comparing with the case of $P_{rot} = 10$ days, it takes more time, $\Delta t_1 + \Delta t_2$, to complete a dynamo loop for the case of $P_{rot} = 25$ days, and hence it has longer cycle period.

In summary, the emergence property of starspots in latitudes plays a crucial role in creating the observed relation between P_{rot} and P_{cyc}. Faster rotators have starspots in closer proximity to the ±55° latitudes, which have the strongest latitudinal differential rotation and, therefore, the highest toroidal field generation efficiency. The strongest latitudinal differential rotation around the ±55° latitudes has been confirmed on the Sun through helioseismology results. Slower rotators with starspots at lower latitudes require extra time to transport and wind up the poloidal flux, resulting in longer cycle periods. As long as the faster rotators have starspots located closer to latitudes of ±55°, the observed $P_{rot} - P_{cyc}$ relation is expected to be reproduced. To verify this deduction, we utilize the equation $n = 9.25(P_{rot}/P_{sun})^2$ to replace Eq. (10). As P_{rot} ranges from 25 days to 10 days, the latitude of maximum α changes from 18° to 40°. The black curves in Figure 7 indicate the simulated relation between P_{rot} and P_{cyc} for dipolar (solid curve) and quadrupolar (dashed curve) solutions. They exhibit similar results as those in Figure 5. On the other hand, the blue curves in Figure 7 show the results for $n = 1$ in Eq. (10), independent of P_{rot}. There is a slight increase in P_{cyc} with the increase of P_{rot}. The increase is too small to account for the observed property. The increase is caused by variations in the meridional flow. Slow rotators have a greater return flow that can transport more toroidal flux towards lower latitudes. This leads to a decrease in the latitude of flux emergence and further a slight increase of the cycle period.

Figures 4 and 5 have shown that for fast rotators ($P_{rot} < 18$ days), the dipolar and quadrupolar modes have the similar cycle periods. And the quadrupolar mode has a smaller α_c, hence is easier to excite. For slow rotators ($P_{rot} \geqslant 18$ days), the dipolar mode has the longer cycle period and is easier to excite than the quadrupolar mode. The time evolution of the quadrupolar field for the cases of $P_{rot} = 10$ days and $P_{rot} = 25$ days is shown in the third and the fourth rows of Fig. 6, respectively. For faster rotators, such as the case of $P_{rot} = 10$ days, the surface poloidal field concentrated around middle-high latitudes. Most equatorward poloidal flux is canceled by the newly generated flux system of a new cycle, also for the toroidal flux. Thus the whole dynamo process operates locally and there are few coupling of magnetic fields between two hemispheres. The degree of the coupling of the poloidal field between two hemispheres determines the parity dominating in the dynamo process (Chatterjee et al. 2004; Hotta & Yokoyama 2010). For slower rotators, such as the case of $P_{rot} = 25$ days, there are the across-equator cancellation of the toroidal field for the dipolar mode. These cancellations entail a longer time for the poloidal flux generation of the new cycle to

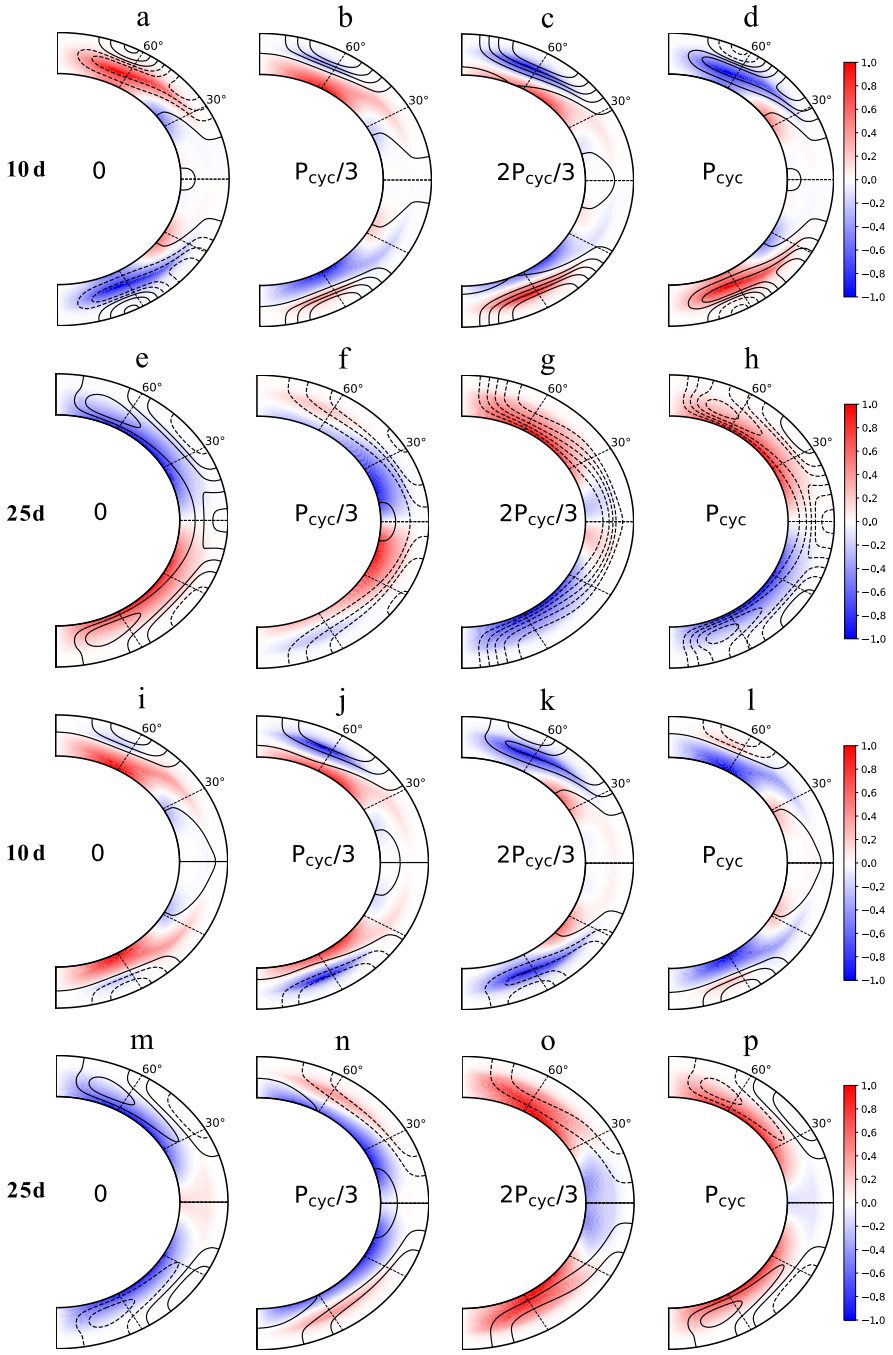

Fig. 6. Snapshots of the magnetic field evolution during the interval of one third of magnetic cycle $P_{cyc}/3$. First (third) row represents rotation period of 10 days with dipolar (quadrupolar) fields. Second (forth) row represents rotation period of 25 days with dipolar (quadrupolar) fields. The strength of magnetic field is arbitrary in a linear regime, and it is normalized to a maximum of 1 here. The region in red (blue) represents toroidal fields inward (outward). The solid (dashed) lines represent the poloidal field clockwise (anticlockwise).

reverse that of the old cycle. The global dipolar mode has the slowest decay in the absence of sources (Cameron et al. 2010). Hence it has a smaller α_c than the quadrupolar mode.

3.2. $P_{rot} - A_{cyc}$ and $P_{rot} - P_{cyc}$ relations in the nonlinear regime

We have investigated the dynamo process in the linear regime and found a dominant role of the starspots' emergence latitudes in determining magnetic cycle. To explore the relation between stars' rotation period P_{rot} and amplitude of stellar activity A_{cyc}, the dynamo model working in the nonlinear regime is required. We adopt the same algebraic quenching term as that in Zhang & Jiang (2022) as the nonlinear amplitude-limitation mechanism here. The initial condition can be any arbitrary linear combinations of the dipolar and quadrupolar field presented by Eqs. (12) and (13), which do not affect the final magnetic field evolution. The strength of the BL source term α_0 is prescribed by Eq. (11)

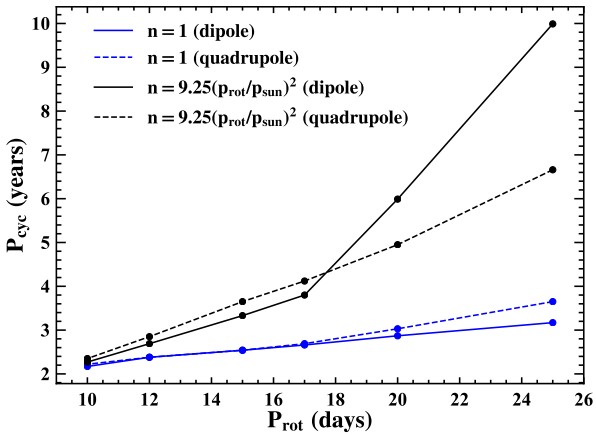

Fig. 7. Relation between rotation period (P_{rot}) and magnetic cycle (P_{cyc}), for cases of n = 1 (blue curve) and n = 9.25$(p_{rot}/p_{sun})^2$ (black curve). The solid (dashed) curve represents the dipolar (quadrupolar) parity solution.

depending on both α_c and P_{rot}, where α_c is set as smaller of α_c^d and α_c^q. Other ingredients of the dynamo model are the same as the one in the linear regime.

In a dynamo model using algebraic quenching, the saturated magnetic field depends on the value $\alpha_0 - \alpha_c$. In this work, we adopt the hypothesis from KN17 to determine α_0 based on α_c and P_{rot}. So an increase of magnetic activity amplitude A_{cyc} with rotation rate P_{rot} is expected, which is demonstrated by Fig. 8. Here magnetic activity amplitude A_{cyc} is measured by cycle-averaged unsigned subsurface toroidal flux, Φ_{tor},

$$\Phi_{tor} = \int_0^{\pi} \int_{0.72R_\odot}^{R_\odot} |B| r \, dr d\theta. \quad (14)$$

For the case of P_{rot} = 25 days, Φ_{tor} is around 10^{23} Mx, which is consistent with observations (Cameron & Schüssler 2015). In contrast, Hazra et al. (2019) show a dip in their $P_{rot} - A_{cyc}$ relation around P_{rot} = 15 days. The dip results from the different ways to deal with the strength of the BL source term α_0. They did not estimate α_c for various rotators. So that the value of $\alpha_0 - \alpha_c$ is not consistent with the expected trend of monotonic increase with the decrease of P_{rot} based on gyrochronology.

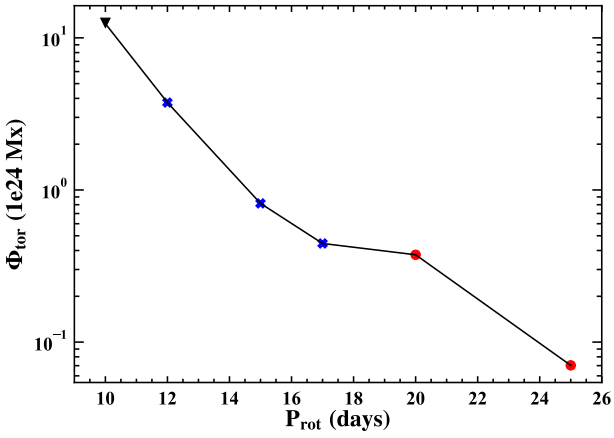

Fig. 8. Relation between rotation period (P_{rot}) and magnetic activity amplitude (A_{cyc}). The activity amplitude is measured by Φ_{tor}. Red dots, blue forks, and black inverted triangle represent the saturated magnetic fields with a dipolar, quadrupolar, and mixed parity, respectively.

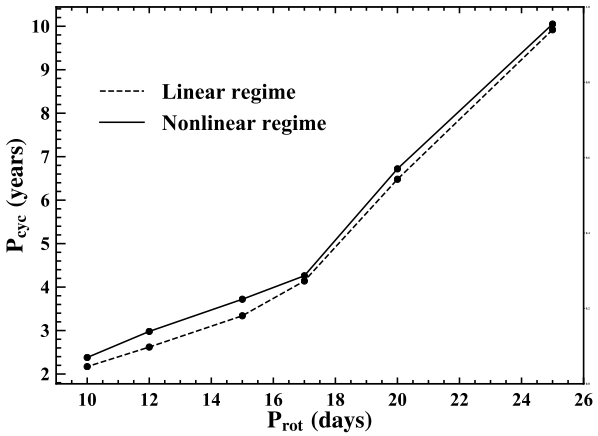

Fig. 9. Relation between rotation period (P_{rot}) and magnetic cycle (P_{cyc}). The solid (dashed) line represents the solution operating in the nonlinear regime (linear regime).

Figure 9 shows the $P_{rot} - P_{cyc}$ relation in both the linear and nonlinear regimes. The magnetic cycles of the nonlinear solutions are slightly longer than that of the linear critical solutions, because algebraic quenching weakens the efficient dynamo number to its critical number as the toroidal field increases (Noyes et al. 1984a; Tobias 1998). We fit the simulated $P_{rot} - P_{cyc}$ relation in the nonlinear regime and obtain $P_{cyc} \propto P_{rot}^{0.85}$, which is close to the observed inactive branch. As demonstrated in the last subsection, the rotation-dependent emergence latitude of starspots is the major reason for our model to reproduce the P_{rot} – P_{cyc} relation, while Hazra et al. (2019) suggested that different profiles of the BL source term had no effect on the P_{rot}–P_{cyc} relation. The two seemingly contradictory statements are caused by two different dynamo models used by the two papers. For Hazra et al. (2019), the toroidal field is mainly generated by the radial shear in the tachocline, which has the strongest value near the poles. Thus although Hazra et al. (2019) adopted two profiles of the BL source term, the surface poloidal field distributions are similar for the two cases they used since the strong toroidal field near the poles dominates the surface poloidal field distributions.

Figure 4 has shown $\alpha_c^d < \alpha_c^q$ for the slowly rotators with $P_{rot} > 18$ days and $\alpha_c^d > \alpha_c^q$ for the fast rotators with $P_{rot} < 18$ days. These indicate that in the weakly nonlinear regime, slowly (fast) rotating stars host dipolar (quadrupolar) global fields. For the case of P_{rot} = 10 days, α_0 is 56% over the critical value according to Eq. (11). The global fields host a mixed parity because the strong super-criticality could lead to the appearance of hemispherically asymmetric mixed mode field (Jennings & Weiss 1991). Figure 10 shows the time-latitude diagram of subsurface toroidal flux (top panels) and surface radial field (bottom panels) for stars with rotation periods of 10, 15, and 25 days. For the case of P_{rot} = 25 days, Figures 10 (e) and (f) well present properties of the solar cycle, such as the dipolar field, regular polar field reversals every about 11 years, and latitudinal migration of the toroidal field. With the decrease of the rotation period from 25 days to 15 days, the surface poloidal field appears at higher latitudes. The magnetic cycle period becomes shorter,

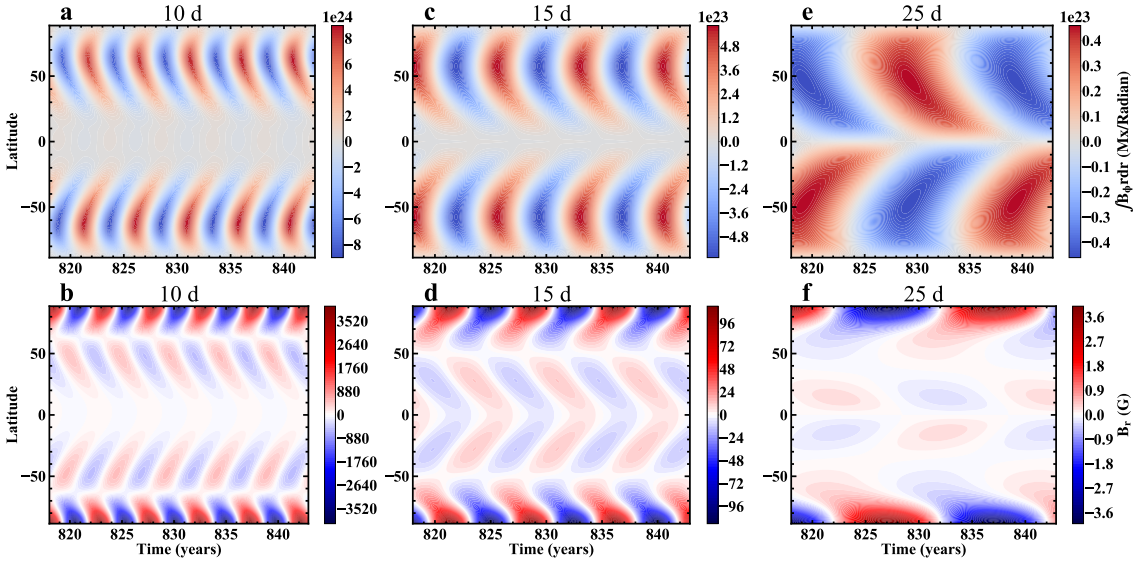

Fig. 10. Time-latitude diagrams of subsurface toroidal flux (top) and surface radial field (bottom) for stars with rotation periods of 10, 15 and 25 days.

activity amplitude is stronger, and the global field shifts to the quadrupolar parity. For the case of P_{rot} = 10 days, Figures 10 (a) and (b) show the mixed-mode solution. Besides the increase of the toroidal flux with the increase of the rotation rate, the amplitude of the polar field also increases with the rotation rate. The trend is consistent with the surface flux transport results given by Schrijver & Title (2001); Işık et al. (2018). The several thousand Gauss polar field could be responsible for the polar starspots in fast rotators.

4. Conclusion and discussion

We have extended the BL mechanism to solar-mass stars and explored the effect of emergence properties of starspots on stellar magnetic cycles. The rotation-dependent emergence latitude and tilt angle of starspots are introduced in a BL-type dynamo working in the bulk of the convection zone developed by Zhang & Jiang (2022). The model accounts well for the observed P_{rot}–P_{cyc} and P_{rot}–A_{cyc} relations about stellar magnetic activity.

We are not the first to extend the BL mechanism developed based on solar observations to understand stellar magnetic cycles. Some efforts had been taken in this direction (e.g., Jouve et al. 2010; Karak et al. 2014b; Kitchatinov & Olemskoy 2015; Vashishth et al. 2023). The past efforts mainly emphasized that the poloidal field results from the tilt angle of starspots and is generated near the stellar surface. The rotation-dependent tilt angle of starspots was considered by Hazra et al. (2019); Kitchatinov (2022). To the best of our knowledge, we are the first to include the rotation-dependent emergence latitude into the BL mechanism to understand stellar cycles. We have also demonstrated that without the rotation-dependent emergence latitude, the resulting P_{rot}–P_{cyc} relation is inconsistent with the observation. The rotation-dependent emergence latitude of starspots is a property presented by observations of stellar magnetic activity. On the other hand, an essential role of the cycle-dependent emergence latitude of sunspots in modulating solar cycles, i.e., latitudinal quenching, was recognized recently (Jiang 2020; Karak 2020). The progress in the understanding of the solar cycle naturally extends to solar-type stars.

Actually some recent studies have focused on effects of the latitudinal distribution and tilt of starspots on stellar magnetic activity, e.g., brightness variations (Işık et al. 2018; Nèmec et al. 2023) and astrometric jitter (Sowmya et al. 2021) based on surface flux transport models (Baumann et al. 2004; Jiang et al. 2014b). The flux emergence properties in latitude and tilt are prescribed by a separate model. These studies assume that different rotators have the same cycle period, i.e., 11 years, as the solar magnetic cycle period. The observed P_{rot}–P_{cyc} relation was not included.

In our BL-type dynamo model, the emergence latitudes of starspots play a crucial role in reproducing the P_{rot}–P_{cyc} relation. Faster rotators have flux emergence closer to ±55° latitudes, where the latitudinal differential rotation and the toroidal field generation efficiency are the strongest. This entails a shorter cycle period. Slower rotators have flux emergence at lower latitudes. It takes some time for the surface poleward meridional flow and turbulent diffusion to transport the emergent poloidal field to around ±55° latitudes. The poloidal flux is transported inwards and equatorward simultaneously. It takes further time for the interior poloidal field at lower latitudes to be wound up to generate a strong enough toroidal field because the lower latitudes have a weaker latitudinal shear. The extra time caused by the surface flux transport and the latitude dependence of the latitudinal shear in the interior leads to the longer cycle period P_{cyc} for slower rotators. There are no strict constraints on the relationship between the emergence latitude and rotation. As long as faster rotators have starspots closer to the ±55° latitudes, the observed P_{rot}–P_{cyc} relation can be reproduced. Without the rotation dependence of the starspots' emergence latitudes, that is n = 1 in Eq. (10), the resulting P_{rot}–P_{cyc} relation is inconsistent with the observed one. The latitude dependence of the latitudinal shear also has a large contribution to the equatorward migration of the toroidal field, i.e., the so-called butterfly diagram (Zhang et al. 2022).

The aforementioned explanations of the observed P_{rot}–P_{cyc} relation based on our BL-type dynamo model discriminate our model developed by Zhang & Jiang (2022) from the flux transport dynamo models (Karak et al. 2014a), in which the equatorward return flow dominates the cycle period and the equatorward migration of the toroidal field. We will analyze the detailed physical ingredients of Zhang & Jiang (2022) accounting for the cycle period and butterfly diagram in a forthcoming paper.

In our BL-type dynamo models, the 55° latitude is regarded as the seat of the stellar dynamo. It is also a key to understanding the P_{rot}–P_{cyc} relation. The essential role of 55° latitude in our dynamo model results from that the toroidal field is generated in the bulk of the convection zone by the latitudinal shear, rather than the widely assumed generation in the tachocline. In the bulk of the convection zone, the 55° latitude has the strongest latitudinal shear. Although few dynamo models emphasize 55° latitude, the importance of 55° latitude in solar magnetism has been addressed by McIntosh et al. (2014, 2021) based on a wide variety of solar observations. The success of our model in reproducing the P_{rot}–P_{cyc} relation of stellar activity adds a new piece of evidence on the important role of 55° latitude in stellar magnetism, and further on the stellar dynamo working in the bulk of the convection zone.

Being different from the P_{rot}–P_{cyc} relation, the P_{rot}–A_{cyc} relation did not pose a challenge for the past attempts to reproduce. For example, Karak et al. (2014b); Kitchatinov & Olemskoy (2015) have explained the relation by taking into account the rotation-dependent tilt angle of starspots in their dynamos. Inspired by KN17 and observations relevant to gyrochronology (Rengarajan 1984; van Saders et al. 2016), we assume that faster-rotating stars operate in a more supercritical regime. The value $\alpha_0 - \alpha_c$, describing how supercritical the dynamo is, is larger for faster rotators. The critical value of the BL source term, α_c, corresponding to the marginal dynamo excitation, is calculated based on the linear models. The larger $\alpha_0 - \alpha_c$ for faster rotators leads to a stronger saturated magnetic field, which explains the P_{rot}–A_{cyc} relation in the nonlinear regime. The large supercriticality corresponding to the strong non-linearity for very fast rotators, e.g., P_{rot} = 10 days, could entail fields with mixed parity. Higher latitude starspots for faster rotators make the coupling of poloidal flux between the two hemispheres more difficult so that the dominated parity for faster rotators could be quadrupolar shifted from the dipolar one for slower rotators. Hazra et al. (2019) have already reported a change in magnetic field parity from dipolar to quadrupolar in rapidly rotating stars. We wait for future stellar magnetic field measurement to verify the shift of magnetic field parity from mixed to quadrupolar, and further to dipolar when a star spins down with age because of the angular momentum loss.

Acknowledgements. Z.Z. and J.J. acknowledge financial support from the National Natural Science Foundation of China through grant Nos. 12173005 and 12350004, and the National Key R&D Program of China No. 2022YFF0503800. L.K. acknowledges financial support from the Ministry of Science and High Education of the Russian Federation.

References

Augustson, K. C., Brown, B. P., Brun, A. S., Miesch, M. S., & Toomre, J. 2012, ApJ, 756, 169
Augustson, K. C., Brun, A. S., & Toomre, J. 2019, ApJ, 876, 83
Baliunas, S. L., Donahue, R. A., Soon, W. H., et al. 1995, ApJ, 438, 269
Balona, L. A. & Abedigamba, O. P. 2016, MNRAS, 461, 497
Barnes, J. R., Collier Cameron, A., Donati, J. F., et al. 2005, MNRAS, 357, L1
Baumann, I., Schmitt, D., Schüssler, M., & Solanki, S. K. 2004, A&A, 426, 1075
Böhm-Vitense, E. 2007, ApJ, 657, 486
Bonanno, A., Elstner, D., Rüdiger, G., & Belvedere, G. 2002, A&A, 390, 673
Boro Saikia, S., Marvin, C. J., Jeffers, S. V., et al. 2018, A&A, 616, A108
Brown, B. P., Browning, M. K., Brun, A. S., Miesch, M. S., & Toomre, J. 2008, ApJ, 689, 1354
Brun, A. S. & Browning, M. K. 2017, Living Reviews in Solar Physics, 14, 4
Brun, A. S., García, R. A., Houdek, G., Nandy, D., & Pinsonneault, M. 2015, Space Sci. Rev., 196, 303
Brun, A. S., Strugarek, A., Noraz, Q., et al. 2022, ApJ, 926, 21
Caligari, P., Moreno-Insertis, F., & Schussler, M. 1995, ApJ, 441, 886
Cameron, R. & Schüssler, M. 2015, Science, 347, 1333
Cameron, R. H., Jiang, J., Schmitt, D., & Schüssler, M. 2010, ApJ, 719, 264
Cameron, R. H., Schmitt, D., Jiang, J., & Işık, E. 2012, A&A, 542, A127
Cameron, R. H. & Schüssler, M. 2017, A&A, 599, A52
Charbonneau, P. 2020, Living Reviews in Solar Physics, 17, 4
Chatterjee, P., Nandy, D., & Choudhuri, A. R. 2004, A&A, 427, 1019
Choudhuri, A. R., Schussler, M., & Dikpati, M. 1995, A&A, 303, L29
Collier Cameron, A. & Donati, J. F. 2002, MNRAS, 329, L23
Dasi-Espuig, M., Solanki, S. K., Krivova, N. A., Cameron, R., & Peñuela, T. 2010, A&A, 518, A7
Dikpati, M. & Charbonneau, P. 1999, ApJ, 518, 508
Do Cao, O. & Brun, A. S. 2011, Astronomische Nachrichten, 332, 907
Durney, B. R. 1995, Sol. Phys., 160, 213
Fan, Y. 2021, Living Reviews in Solar Physics, 18, 5
Güdel, M. 2004, A&A Rev., 12, 71
Guerrero, G. & de Gouveia Dal Pino, E. M. 2008, A&A, 485, 267
Guerrero, G., Zaire, B., Smolarkiewicz, P. K., et al. 2019, ApJ, 880, 6
Hathaway, D. H. 2015, Living Reviews in Solar Physics, 12, 4
Hazra, G., Jiang, J., Karak, B. B., & Kitchatinov, L. 2019, ApJ, 884, 35
Hazra, G., Karak, B. B., & Choudhuri, A. R. 2014, ApJ, 782, 93
Hazra, S. & Nandy, D. 2016, ApJ, 832, 9
Hempelmann, A., Schmitt, J. H. M. M., & Stępień, K. 1996, A&A, 305, 284
Hotta, H. & Yokoyama, T. 2010, ApJ, 714, L308
Işık, E., Solanki, S. K., Krivova, N. A., & Shapiro, A. I. 2018, A&A, 620, A177
Jennings, R. L. & Weiss, N. O. 1991, MNRAS, 252, 249
Jiang, J. 2020, ApJ, 900, 19
Jiang, J., Cameron, R. H., Schmitt, D., & Işık, E. 2013, A&A, 553, A128
Jiang, J., Cameron, R. H., Schmitt, D., & Schüssler, M. 2011, A&A, 528, A82
Jiang, J., Cameron, R. H., & Schüssler, M. 2014a, ApJ, 791, 5
Jiang, J., Hathaway, D. H., Cameron, R. H., et al. 2014b, Space Sci. Rev., 186, 491
Jiang, J. & Wang, J.-X. 2006, Chinese J. Astron. Astrophys., 6, 227
Jiang, J. & Wang, J. X. 2007, MNRAS, 377, 711
Jiang, J., Wang, J.-X., Jiao, Q.-R., & Cao, J.-B. 2018, ApJ, 863, 159
Jiao, Q., Jiang, J., & Wang, Z.-F. 2021, A&A, 653, A27
Jouve, L., Brown, B. P., & Brun, A. S. 2010, A&A, 509, A32
Jouve, L. & Brun, A. S. 2007, A&A, 474, 239
Jouve, L., Brun, A. S., Arlt, R., et al. 2008, A&A, 483, 949
Karak, B. B. 2010, ApJ, 724, 1021
Karak, B. B. 2020, ApJ, 901, L35
Karak, B. B., Jiang, J., Miesch, M. S., Charbonneau, P., & Choudhuri, A. R. 2014a, Space Sci. Rev., 186, 561
Karak, B. B., Kitchatinov, L. L., & Choudhuri, A. R. 2014b, ApJ, 791, 59
Kitchatinov, L. 2022, Research in Astronomy and Astrophysics, 22, 125006
Kitchatinov, L. & Nepomnyashchikh, A. 2017a, MNRAS, 470, 3124
Kitchatinov, L. L. & Nepomnyashchikh, A. A. 2017b, Astronomy Letters, 43, 332
Kitchatinov, L. L. & Olemskoy, S. V. 2011, MNRAS, 411, 1059
Kitchatinov, L. L. & Olemskoy, S. V. 2012, MNRAS, 423, 3344
Kitchatinov, L. L. & Olemskoy, S. V. 2015, Research in Astronomy and Astrophysics, 15, 1801
Kitchatinov, L. L. & Rüdiger, G. 1999, A&A, 344, 911
Kochukhov, O. 2021, A&A Rev., 29, 1
Li, K. J., Wang, J. X., Zhan, L. S., et al. 2003, Sol. Phys., 215, 99
McIntosh, S. W., Leamon, R. J., Egeland, R., et al. 2021, Sol. Phys., 296, 189
McIntosh, S. W., Wang, X., Leamon, R. J., et al. 2014, ApJ, 792, 12
Montet, B. T., Tovar, G., & Foreman-Mackey, D. 2017, ApJ, 851, 116
Muñoz-Jaramillo, A., Nandy, D., & Martens, P. C. H. 2011, ApJ, 727, L23
Muñoz-Jaramillo, A., Dasi-Espuig, M., Balmaceda, L. A., & DeLuca, E. E. 2013, The Astrophysical Journal Letters, 767, L25
Nandy, D. 2004, Sol. Phys., 224, 161
Nelson, N. J., Brown, B. P., Brun, A. S., Miesch, M. S., & Toomre, J. 2013, ApJ, 762, 73
Nèmec, N. E., Shapiro, A. I., Işık, E., Solanki, S. K., & Reinhold, T. 2023, A&A, 672, A138
Noyes, R. W., Hartmann, L. W., Baliunas, S. L., Duncan, D. K., & Vaughan, A. H. 1984a, ApJ, 279, 763
Noyes, R. W., Weiss, N. O., & Vaughan, A. H. 1984b, ApJ, 287, 769
Parker, E. N. 1955, ApJ, 121, 491
Petrovay, K., Nagy, M., & Yeates, A. R. 2020, Journal of Space Weather and Space Climate, 10, 50
Pipin, V. V. & Kosovichev, A. G. 2016, ApJ, 823, 133
Reinhold, T., Cameron, R. H., & Gizon, L. 2017, A&A, 603, A52
Rengarajan, T. N. 1984, ApJ, 283, L63
Saar, S. H. & Brandenburg, A. 1999, ApJ, 524, 295
Schou, J., Antia, H. M., Basu, S., et al. 1998, ApJ, 505, 390
Schrijver, C. J., Shine, R. A., Hagenaar, H. J., et al. 1996, ApJ, 468, 921
Schrijver, C. J. & Title, A. M. 2001, ApJ, 551, 1099
Schuessler, M. & Solanki, S. K. 1992, A&A, 264, L13
Solanki, S. K., Wenzler, T., & Schmitt, D. 2008, A&A, 483, 623
Sowmya, K., Nèmec, N. E., Shapiro, A. I., et al. 2021, ApJ, 919, 94

Strassmeier, K. G. 2009, A&A Rev., 17, 251
Strassmeier, K. G., Rice, J. B., Wehlau, W. H., et al. 1991, A&A, 247, 130
Strugarek, A., Beaudoin, P., Charbonneau, P., Brun, A. S., & do Nascimento, J. D. 2017, Science, 357, 185
Talafha, M., Nagy, M., Lemerle, A., & Petrovay, K. 2022, A&A, 660, A92
Tobias, S. M. 1998, MNRAS, 296, 653
van der Houwen, P. J. & Sommeijer, B. P. 2001, Journal of Computational and Applied Mathematics, 128, 447
van Saders, J. L., Ceillier, T., Metcalfe, T. S., et al. 2016, Nature, 529, 181
Vashishth, V., Karak, B. B., & Kitchatinov, L. 2023, MNRAS, 522, 2601
Vogt, S. S. & Penrod, G. D. 1983, PASP, 95, 565
Wang, Y. M., Sheeley, N. R., J., & Nash, A. G. 1991, ApJ, 383, 431
Wang, Y. M. & Sheeley, N. R. 2002, Journal of Geophysical Research (Space Physics), 107, 1302
Warnecke, J. 2018, A&A, 616, A72
Wilson, O. C. 1978, ApJ, 226, 379
Wright, N. J. & Drake, J. J. 2016, Nature, 535, 526
Wright, N. J., Drake, J. J., Mamajek, E. E., & Henry, G. W. 2011, ApJ, 743, 48
Yadav, R. K., Gastine, T., Christensen, U. R., & Reiners, A. 2015, A&A, 573, A68
Zhang, J., Bi, S., Li, Y., et al. 2020, ApJS, 247, 9
Zhang, Z. & Jiang, J. 2022, ApJ, 930, 30
Zhang, Z., Jiang, J., & Zhang, H. 2022, ApJ, 941, L3